2007 IEEE International Conference on
Robotics and Automation
Roma, Italy, 10-14 April 2007

On Motion Planning for Ball-Plate Systems With Limited Contact Area

Mikhail Svinin and Shigeyuki Hosoe

Abstract— **The paper deals with motion planning for rolling-based systems with limited contact area. In a simplified formulation, the driving principle for such systems is based on controlling the position of the center of mass of the object, exploiting non-holonomic rolling constraint to propel the hemisphere. Two geometric algorithms for motion planning are formulated, analyzed, and tested under simulation. The simulation results show the possibility of moving the system to the desired configurations by steering the contact point on the hemisphere by generalized figure eights represented by circles and Viviani's curves.**

I. Introduction

In recent years there appears an interest to robotic systems where non-holonomic rolling constraints are used not only for manipulation but also for locomotion. In such systems self-propelled movements are usually generated by creating imbalance and changing the system inertia. An example of such systems is a spherical mobile robot [1], [2]. Similar robotic systems were considered in [3] and [4]. Also of interest is the study on legless locomotion [5], [6], showing practical applications in situations where a walking machine, having a spherical body, becomes limited in the ability to use its legs.

Our interest to rolling-based locomotion is motivated by highly skillful movements observed in human beings and animals (see Figure 1). To imitate this type of movements, one can place a robotic mechanism on a spherical object. This system, however, would be extremely complex for an initial study, and it could be reasonable to resort to simplifications shown in Figure 1. In the simplified formulation we deal with a hemisphere and replace the robot by its center of masses projected on the main hemisphere plane. The driving principle is then based on controlling the position of the center of mass of the robot, exploiting non-holonomic rolling constraint to propel the object.

One of the key problems in the control of non-holonomic systems with rolling constraints, such as a ball-plate system, is the construction of motion planning algorithms. The problem is challenging because even though the ball-plate system is controllable [7], it cannot be represented in chained form, is not differentially flat, and is not nilpotent [8]. One can divide the existing approaches to motion planning for the ball-plate system into two directions. The first one is based on a proper control parameterization [9]–[11], while the second deals with the geometric phases [7], [12]. In the geometric phase approaches a closed path of the control inputs results in a change of the contact coordinates. For the ball-plate system it was first outlined in [7] and revisited in [13]. Motion planning for a general surface in contact with a plane was proposed in [14], [15] and later on was generalized to the case of polyhedra [16].

M. Svinin and S. Hosoe are with Bio-Mimetic Control Research Center, RIKEN, Anagahora, Shimoshidami, Moriyama-ku, Nagoya, Aichi 463-0003, Japan svinin(hosoe)@bmc.riken.jp

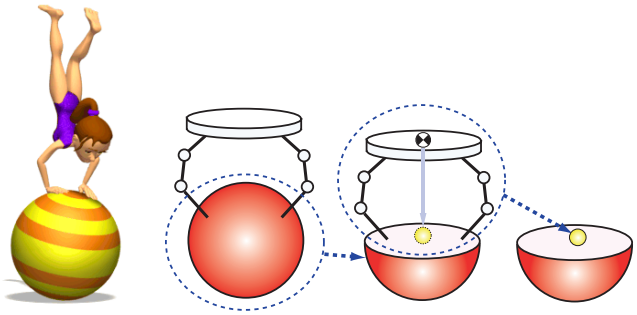

Fig. 1. Motivating example and simplification of the control problem.

Our study was inspired initially by the research on rolling-based manipulation introduced in [17], where the motion planning was based on the construction of a set of multiple spherical triangles on the object surface. Also relevant to our research are the studies reported in [18] and [19], where planning algorithms utilizing geodesic quadrilaterals were proposed. These algorithms produce piecewise smooth trajectories, but the motion of the system needs to be stopped at the vertexes of the spherical polygons. To increase the smoothness of the planned trajectories, a circle-based planning technique was introduced in [20]. This technique, in turn, can be generalized further to produce even smoother trajectories, and this constitutes the main goal of our paper.

This paper is organized as follows. In Section II we sketch a model of the ball-plate system and fix the notation. A simplified formulation of the motion planning problem is addressed in Section III. There, we first review the circle-based planning technique [20] and then show that the continuous trajectories in the time domain can be constructed only up to given order of the highest continuous derivative. To be able to generate C^∞ trajectories, we then propose an algorithm based on tracing the generalized Viviani curves and test it under simulation. Finally, conclusions are summarized in Section IV.

II. Mathematical Model

To describe the system under consideration, we introduce the following coordinate frames (see Figure 2): Σ_b is an inertial frame fixed at the base, Σ_o is a frame fixed at the geometric center of the object (hemisphere), Σ_a is a frame

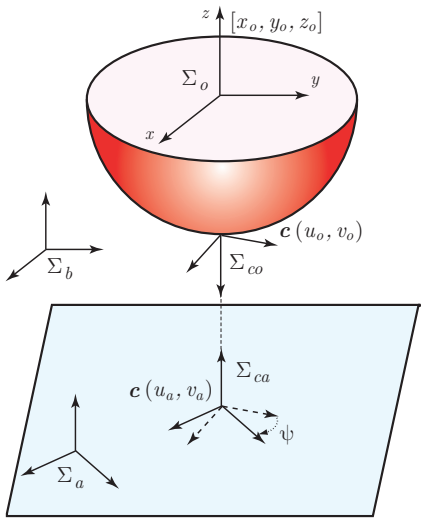

Fig. 2. System formalization.

fixed at the contact plane. In addition, at the contact point we introduce the contact frame of the object Σ_{co}, and the contact frame of the plane, Σ_{ca}.

The contact coordinates are given by the vectors $\boldsymbol{u}_{co} = [u_o, v_o]^{\mathrm{T}}$, expressing the contact point on the hemisphere surface, $\boldsymbol{u}_{ca} = [u_a, v_a]^{\mathrm{T}}$, expressing the contact point on the plane, and by the contact angle ψ which is defined as the angle between the x-axis of Σ_{co} and Σ_{ca}. The orientation of the x- and y-axes of Σ_{co} relative to the x- and y-axes of Σ_{ca} is defined by the matrix

$$\mathcal{R}_\psi = \begin{bmatrix} -\cos\psi & \sin\psi \\ \sin\psi & \cos\psi \end{bmatrix}. \tag{1}$$

The position of a point on the sphere is parameterized as

$$\boldsymbol{c}(u_o, v_o) = R \begin{bmatrix} -\sin u_o \cos v_o \\ \sin v_o \\ -\cos u_o \cos v_o \end{bmatrix}. \tag{2}$$

In this parameterization the origin is placed at the south pole of the sphere. The lower hemisphere is selected by imposing $-\pi/2 < u_o < \pi/2$ and $-\pi/2 < v_o < \pi/2$.

Under the assumption of pure rolling, the contact kinematic equations can be represented as [12], [21]

$$\dot{u}_a = -R\cos\psi\cos v_o\,\dot{u}_o + R\sin\psi\,\dot{v}_o, \tag{3}$$
$$\dot{v}_a = R\sin\psi\cos v_o\,\dot{u}_o + R\cos\psi\,\dot{v}_o, \tag{4}$$
$$\dot{\psi} = \sin v_o\,\dot{u}_o. \tag{5}$$

III. Motion Planning

In this section we deal with the motion planning problem in a simplified formulation. Namely, we assume that at the start and end configurations the initial and final values of $\boldsymbol{u}_{co}$ are zero. The assumption restricts the generality[1] but is natural for the systems of our interest.

[1]However, the algorithms proposed in section can constitute a kernel part of a more general three stage manipulation strategy, similar to that outlined in [7] and [13], if they are accompanied by two trivial maneuvers.

A. Trajectory planning using circles

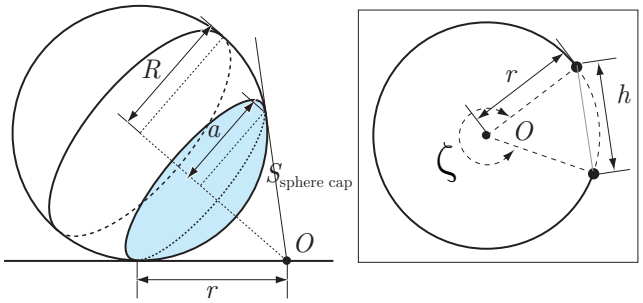

Fig. 3. Circular movement on the sphere (left) and on the plane (right).

1) Basic considerations and algorithm [20]: Draw a circle of the radius a on the sphere as shown in Figure 3. The trajectory of the contact point on the plane, corresponding to the circle on the sphere, is a circular arc of the radius

$$r(a) = \frac{a}{\sqrt{1-(a/R)^2}}, \tag{6}$$

with the central angle

$$\zeta(a) = 2\pi\sqrt{1-(a/R)^2}. \tag{7}$$

The displacement of the contact point h is defined as

$$h(a) = 2r(a)\sin(\zeta(a)/2), \tag{8}$$

the change of the relative angle is

$$\delta\psi(a) = 2\pi\left(1-\sqrt{1-(a/R)^2}\right). \tag{9}$$

A combination of two circles of radii a and b, taken with opposite direction of rotation, is called a movement step. The two circles have a common tangent line. The total linear displacement of the contact point for one movement step and the change of the relative angle are given by

$$h(a,b) = \sqrt{h^2(a)+h^2(b)+2h(a)h(b)\cos\left(\frac{\zeta(a)-\zeta(b)}{2}\right)}, \tag{10}$$
$$\eta(a,b) = \delta\psi(a) - \delta\psi(b) = \zeta(b) - \zeta(a). \tag{11}$$

Assume that the motion from the initial to the final configuration is composed of n movement steps as shown Figure 4. Then,

$$\eta(a,b) = \psi_{des}/n, \tag{12}$$

where ψ_{des} is the desired orientation. The total displacement is defined as

$$\boldsymbol{d} = \sum_{k=0}^{n-1} \overrightarrow{P_k P_{k+1}}. \tag{13}$$

To calculate the traveling distance $|\boldsymbol{d}|$, introduce local frames associated with each movement steps as shown in Figure 4. The projection of the vector $\boldsymbol{d}$ in the axes of Σ_a and in the axes of the frame associated with the initial movement step are denoted as, respectively, $\boldsymbol{d}^{(a)}$ and $\boldsymbol{d}^{(0)}$. They are related as

$$\boldsymbol{d}^{(a)} = R_z(\theta)\boldsymbol{d}^{(0)}, \tag{14}$$

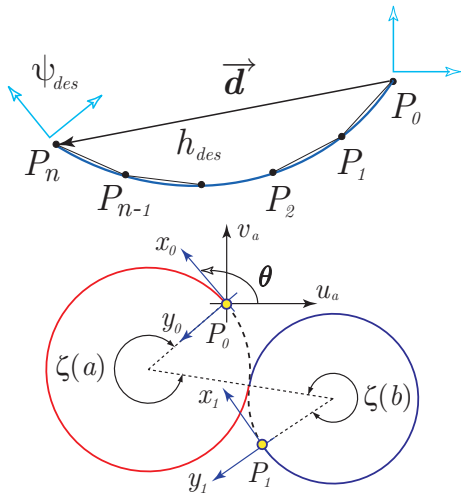

Fig. 4. n-step movement and initial orientation.

where

$$R_z(\theta) \triangleq \begin{bmatrix} \cos\theta & -\sin\theta \\ \sin\theta & \cos\theta \end{bmatrix}, \tag{15}$$

and θ is the angle defining the orientation of the initial tangent line, which is unknown at the moment. It is adjusted later on from the requirement that the vector of the resulting displacement should point to the desired destination.

The mutual orientation of the two adjacent local frames is defined by the angle $\eta(a,b)$. Expressing (13) in the axes of the initial local frame, one obtains

$$\boldsymbol{d}^{(0)} = \sum_{k=0}^{n-1} R_z^k(\eta(a,b))\overrightarrow{P_0P_1^{(0)}} \triangleq \mathcal{R}(n,\eta)\,\overrightarrow{P_0P_1^{(0)}}, \tag{16}$$

where

$$\mathcal{R}(n,\eta)=\begin{bmatrix} 1+\dfrac{\cos\frac{n\eta}{2}\sin\frac{(n-1)\eta}{2}}{\sin\frac{\eta}{2}} & -\dfrac{\sin\frac{n\eta}{2}\sin\frac{(n-1)\eta}{2}}{\sin\frac{\eta}{2}} \\ \dfrac{\sin\frac{n\eta}{2}\sin\frac{(n-1)\eta}{2}}{\sin\frac{\eta}{2}} & 1+\dfrac{\cos\frac{n\eta}{2}\sin\frac{(n-1)\eta}{2}}{\sin\frac{\eta}{2}} \end{bmatrix}. \tag{17}$$

Taking into account that $|\overrightarrow{P_0P_1^{(0)}}| = h(a,b)$ and $\mathcal{R}^{\mathrm{T}}\mathcal{R} = \boldsymbol{I}\sin^2(n\,\eta/2)/\sin^2(\eta/2)$, where $\boldsymbol{I}$ is the identity matrix, from the condition $|\boldsymbol{d}^{(0)}| = h_{des}$ one obtains

$$h(a,b) = \frac{\sin(\psi_{des}/2n)}{\sin(\psi_{des}/2)}h_{des}. \tag{18}$$

Now, given $h_{des}, \psi_{c_{des}}$, and the number of movement steps, n, one can obtain a and b from solving (12) and (18). Finally, having established a and b, one can define the orientation of the starting tangent line. By setting in (14) $\boldsymbol{d}^{(a)} = \boldsymbol{d}_{des}$ and calculating $\boldsymbol{d}^{(0)}(a,b)$, the angle θ between $\boldsymbol{d}^{(0)}$ and $\boldsymbol{d}_{des}$ is obtained as

$$\theta = \arccos\frac{\boldsymbol{d}^{(0)}\cdot\boldsymbol{d}_{des}}{h_{des}^2}. \tag{19}$$

2) Simulation example: In the simulation, the initial contact point coordinates are $\boldsymbol{u}_{co} = [0,0]^{\mathrm{T}}(\mathrm{rad})$, $\boldsymbol{u}_{ca} = [0,0]^{\mathrm{T}}(\mathrm{m})$, and the initial relative angle ψ is 0 rad. The desired contact point coordinates are set as $\boldsymbol{u}_{co} = [0,0]^{\mathrm{T}}(\mathrm{rad})$, $\boldsymbol{u}_{ca} = [0.2,0.3]^{\mathrm{T}}(\mathrm{m})$, and the desired relative angle ψ is $\pi/6$ rad. The radius of the hemisphere is 0.2m. Here we set $n=4$ and obtain $a = 0.0846\mathrm{m}$, $b = 0.0751\mathrm{m}$ from solving equations (12,18). The turning angle $\theta = -1.6410(\mathrm{rad})$ is obtained from (19). The evolution of the contact point on the contact plane and on the hemisphere in shown in Figure 5. Note that the whole maneuver is executed by generating only two circles on the hemisphere.

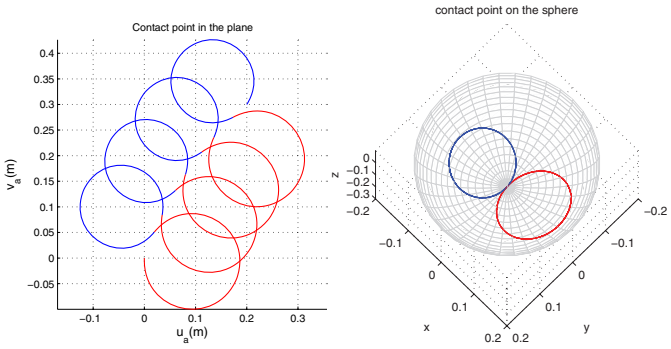

Fig. 5. Trajectory of the contact point on the plane (left) and on the sphere (right); 1st half-step is shown in red, while 2nd in blue color.

3) Trajectory formation in the time domain: Let us consider now the construction of motion trajectories in the time domain. For this purpose the position of the contact point in the contact plane can be parameterized by the arc angle φ. For the first half-step, where $\varphi \in [0,\zeta(a)]$, we have

$$\boldsymbol{u}_{ca,k}^{(0)} = \mathcal{R}(k-1,\eta)\overrightarrow{P_0P_1^{(0)}} + R_z((k-1)\eta)r(a)\begin{bmatrix}\sin\varphi \\ 1-\cos\varphi\end{bmatrix}, \tag{20}$$

and for the second half-step, where we set $\varphi \in [\zeta(b),0]$,

$$\boldsymbol{u}_{ca,k}^{(0)} = \mathcal{R}(k,\eta)\overrightarrow{P_0P_1^{(0)}} - R_z(k\eta)r(b)\begin{bmatrix}\sin\varphi \\ 1-\cos\varphi\end{bmatrix}. \tag{21}$$

In practical implementation the angle φ can be specified, for instance, by polynomials of time. The trajectory planning in the time domain is then reduced to a spline interpolation. To do so, we have to specify the boundary conditions for the angle φ and its derivatives at the interior points, which are the points of connection of the half-steps of the circular movements.

Differentiating (20,21), one obtains the velocities

$$\dot{\boldsymbol{u}}_{ca,k}^{(0)} = \begin{cases} R_z((k-1)\eta)r(a)\begin{bmatrix}\cos\varphi \\ \sin\varphi\end{bmatrix}\dot{\varphi}, & \varphi\in[0,\zeta(a)], \\ -R_z(k\eta)r(b)\begin{bmatrix}\cos\phi \\ \sin\phi\end{bmatrix}\dot{\varphi}, & \varphi\in[\zeta(b),0], \end{cases} \tag{22}$$

and the accelerations of the contact point

$$\ddot{\boldsymbol{u}}^{(0)}_{ca,k} = \begin{cases} R_z((k-1)\eta)r(a)\left(\begin{bmatrix}\cos\varphi\\ \sin\varphi\end{bmatrix}\ddot{\varphi}+\begin{bmatrix}-\sin\varphi\\ \cos\varphi\end{bmatrix}\dot{\varphi}^2\right) \\ -R_z(k\eta)r(b)\left(\begin{bmatrix}\cos\varphi\\ \sin\varphi\end{bmatrix}\ddot{\varphi}+\begin{bmatrix}-\sin\varphi\\ \cos\varphi\end{bmatrix}\dot{\varphi}^2\right) \end{cases}. \tag{23}$$

Similar expressions can be obtained for the higher derivatives. It is easy to show that in order to guarantee the continuity of the velocities at the points of connections between the first and second half-steps one needs to impose the following condition

$$r(a)\dot{\varphi}_a + r(b)\dot{\varphi}_b = 0. \tag{24}$$

The conditions for the continuity of the accelerations are defined as

$$r(a)\ddot{\varphi}_a + r(b)\ddot{\varphi}_b = 0, \tag{25}$$
$$r(a)\dot{\varphi}_a^2 + r(b)\dot{\varphi}_b^2 = 0. \tag{26}$$

Thus, the continuity of the accelerations requires zero instantaneous velocity at the connection point.

The discussion can be easily extended to the analysis of the higher derivatives. In particular, it can be shown that the continuity of the jerks reduces to the following conditions

$$r(a)(\dddot{\varphi}_a - \dot{\varphi}_a^3) + r(b)(\dddot{\varphi}_b - \dot{\varphi}_b^3) = 0, \tag{27}$$
$$3r(a)\dot{\varphi}_a\ddot{\varphi}_a + 3r(b)\dot{\varphi}_b\ddot{\varphi}_b = 0. \tag{28}$$

Providing that the velocities and accelerations are continuous, these conditions are further reduced to

$$r(a)\dddot{\varphi}_a + r(b)\dddot{\varphi}_b = 0. \tag{29}$$

Similarly, the continuity of the snaps requires

$$r(a)(\ddddot{\varphi}_a - 6\dot{\varphi}_a\ddot{\varphi}) + r(b)(\ddddot{\varphi}_b - 6\dot{\varphi}\ddot{\varphi}) = 0, \tag{30}$$
$$r(a)(4\dot{\varphi}_a\dddot{\varphi}_a + 3\ddot{\varphi}_a^2 - \dot{\varphi}_a^4) + r(b)(4\dot{\varphi}_a\dddot{\varphi}_a + 3\ddot{\varphi}_a^2 - \dot{\varphi}_a^4) = 0. \tag{31}$$

Providing that the velocities, accelerations and jerks are continuous, these conditions are reduced to

$$r(a)\ddddot{\varphi}_a + r(b)\ddddot{\varphi}_b = 0. \tag{32}$$

The generalization of this discussion is straight-forward. In particular, it is clear that it is impossible to construct C^∞ trajectories in the time domain. However, we can construct the continuous trajectories up to a given order of the highest continuous derivative.

Consider first the specification of $\varphi(t)$ by 3rd order polynomials. Here, in addition to the two matching conditions $\varphi_a(t_c) = \zeta(a)$ and $\varphi_b(t_c) = \zeta(b)$, two more conditions need to be specified at the interior points. The trivial choice of $\dot{\varphi}_a(t_c) = \dot{\varphi}_a(t_c) = 0$ leads to the conventional minimum acceleration type of parameterization. Instead of that one can impose the conditions (24,25). The circle connection points will then be passed with non-zero velocities but the accelerations will not be continuous because the condition (26) is not satisfied. Physically, the radial component of the acceleration of the contact point will change the sign to the opposite at the connection moment t_c.

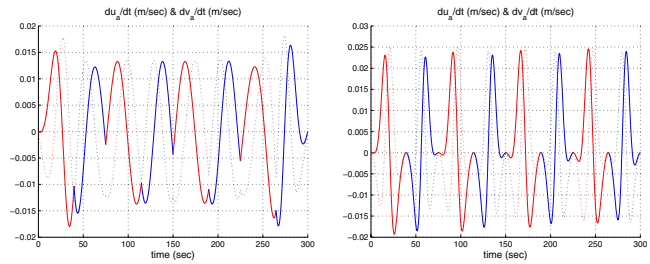

Fig. 6. Velocity of the contact point on the contact plane as functions of time under parameterization by 3rd (left) and 5th (right) order polynomials. Solid lines correspond to $u_a(t)$ while dotted lines do to $v_a(t)$. Red color correspond to the 1st half-step, while blue to the 2nd.

Consider next the specification of $\varphi(t)$ by 5th order polynomials. Here, in addition to the two matching conditions $\varphi_a(t_c) = \zeta(a)$ and $\varphi_b(t_c) = \zeta(b)$, four more conditions need to be specified at the interior points. The trivial choice of $\dot{\varphi}_a(t_c) = \dot{\varphi}_a(t_c) = 0$ and $\ddot{\varphi}_a(t_c) = \ddot{\varphi}_a(t_c) = 0$ leads to the conventional minimum jerk type of parameterization. Instead of that one can impose the conditions (24,25) and (29,32). The circle connection points will then be passed with zero instantaneous velocities but non-zero accelerations. Interestingly, in this method the derivatives of the contact point up to the 4th order will be continuous functions of time. Simulation results for the example considered in Section III-A.2 are illustrated in Figure 6.

B. Trajectory planning using generalized Viviani's curve

The simulation results in Section III-A.2 hint at the idea that the steering of the system under consideration can be implemented in a hula hoop manner. In this connection the motion planning problem can be reformulated in the following way. Given a smooth figure eight on the hemisphere, find the sizes of its two ovals that brings the system to the desired configuration.

1) Basic considerations: As a candidate for the figure eight one can use Viviani's curve. This is the curve of intersection of the surfaces of a sphere of radius R and a circular cylinder of radius $R-d$ tangent to the inner surface of the sphere. A parameterization of this curve suitable for our problem (setting the tangent plane of the cylinder and the sphere to be the contact plane) can be defined as

$$\boldsymbol{c}(\varphi) = \begin{bmatrix} 2\sqrt{d(R-d)}\sin(\varphi/2) \\ (d-R)\sin\varphi \\ -d + (d-R)\cos\varphi \end{bmatrix}, \tag{33}$$

where $\varphi \in [0, 4\pi]$. The classical Viviani curve is defined for $d = R/2$. The orthogonal projection of this curve on the contact plane defines the lemniscate of Gerono, while the stereographic projection defines the lemniscate of Bernoulli. This curve is periodic. Since this curve and its derivatives are well defined for any φ, there will be no problem in constructing C^∞ parameterization in the time domain.

Note that the curve (33) is symmetric which is not suitable for our steering strategy. To make (33) asymmetric, we define

$$d = a - b\sin(\varphi/2). \tag{34}$$

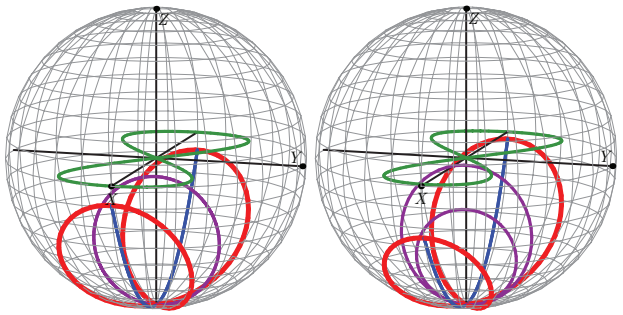

Fig. 7. Symmetric and asymmetric Viviani's curves (red color) and their projections on the coordinate planes.

The symmetric and asymmetric Viviani curves are shown in Fig. 7. The constraints on the parameter a and b are defined from the condition $R/2 < d < R$, which translates to the following inequalities

$$1/2 < \frac{a}{R} < 1, \quad \left|\frac{b}{R}\right| < 1 - \frac{a}{R}, \quad \left|\frac{b}{R}\right| < \frac{a}{R} - \frac{1}{2}. \qquad (35)$$

In general, however, it is not enough to impose these conditions to produce well-defined figure eights. It is possible to show that a well-defined parameterization is obtained if we restrict the parameters in such a way so that the vector of the second derivatives of (33) at the "east" ($\varphi = 3\pi$) and "west" ($\varphi = \pi$) points is directed to the center ($\varphi = 0$). These conditions translate to the following inequalities

$$3\frac{b}{R} + 2\frac{a}{R} - 4\frac{b^2}{R^2} - 6\frac{ab}{R^2} - 2\frac{a^2}{R^2} > 0, \qquad (36)$$

$$3\frac{b}{R} - 2\frac{a}{R} + 4\frac{b^2}{R^2} - 6\frac{ab}{R^2} + 2\frac{a^2}{R^2} < 0, \qquad (37)$$

which define hyperbolic lines in the parameter plane a, b. The construction of the admissible area for the parameters a and b is shown in Fig. 8.

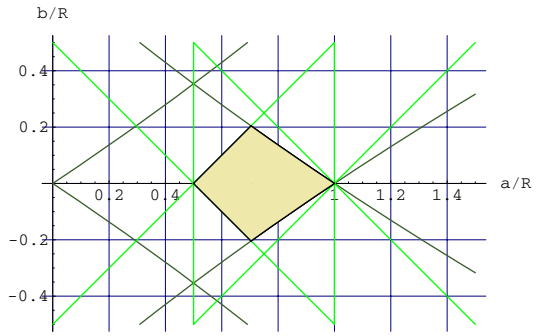

Fig. 8. Admissible area for the parameters a and b. Light green lines correspond to (35), and dark green lines correspond to (36,37).

2) Algorithm: The construction of the motion planning algorithm based on the Viviani curves is conceptually similar to the circle-based planning. Namely, we need to solve equations (12,18) and define the parameters a and b. However, now the closed form expressions for $h(a,b)$ and $\eta(a,b)$ are not available and need to be established numerically. Taking into account that

$$\dot{u}_o = \frac{1}{R^2\cos^2 v_o}\boldsymbol{c}_u^{\mathrm{T}}\boldsymbol{c}_\varphi\dot{\varphi}, \qquad (38)$$

$$\dot{v}_o = \frac{1}{R^2}\boldsymbol{c}_v^{\mathrm{T}}\boldsymbol{c}_\varphi\dot{\varphi}, \qquad (39)$$

we obtain from (3-5)

$$\partial u_a/\partial\varphi = -\frac{\cos\psi}{R\cos v_o}\boldsymbol{c}_u^{\mathrm{T}}\boldsymbol{c}_\varphi + \frac{\sin\psi}{R}\boldsymbol{c}_v^{\mathrm{T}}\boldsymbol{c}_\varphi, \qquad (40)$$

$$\partial v_a/\partial\varphi = \frac{\sin\psi}{R\cos v_o}\boldsymbol{c}_u^{\mathrm{T}}\boldsymbol{c}_\varphi + \frac{\cos\psi}{R}\boldsymbol{c}_v^{\mathrm{T}}\boldsymbol{c}_\varphi, \qquad (41)$$

$$\partial\psi/\partial\varphi = \frac{\sin v_o}{R^2\cos^2 v_o}\boldsymbol{c}_u^{\mathrm{T}}\boldsymbol{c}_\varphi. \qquad (42)$$

Here, $\boldsymbol{c}_u = \partial\boldsymbol{c}/\partial u_o$ and $\boldsymbol{c}_v = \partial\boldsymbol{c}/\partial v_o$ are defined from (2), and $\boldsymbol{c}_\varphi = \partial\boldsymbol{c}/\partial\varphi$ is defined from (33). Integrating (40-42) for one step of movement ($\varphi \in [0, 4\pi]$) with zero initial conditions, we define $h(a,b) \triangleq \sqrt{u_a^2(4\pi) + v_a^2(4\pi)}$ and $\eta(a,b) \triangleq \psi(4\pi)$.

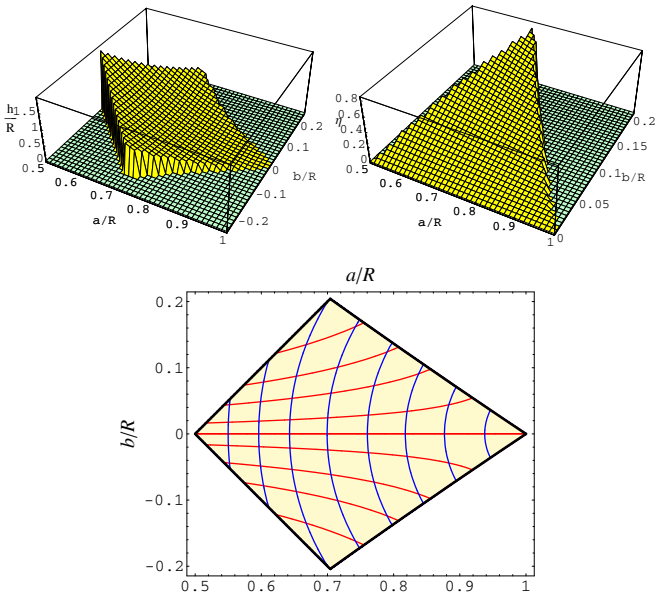

Fig. 9. Normalized non-holonomic shift $h(a,b)/R$ (top left) and phase change $\eta(a,b)$ (top right) as functions of a/R and b/R. Contour lines of $h(a,b)/R$ (blue) and $\eta(a,b)$ (red) are shown in the bottom part.

It can be deduced from geometric considerations that the non-holonomic shift is symmetric with respect to the parameter b, $h(a,b) = h(a,-b)$, while the phase change is asymmetric, $\eta(a,b) = -\eta(a,-b)$. The functions $h(a,b)$ and $\eta(a,b)$ are shown in Fig. 9. Providing that ψ_{des}/n and $h_{des}\sin(\psi_{des}/2n)/\sin(\psi_{des}/2)$ are in the proper range, the solution for a and b is established uniquely. This conclusion can be easily established from Fig. 9 (a level line for the surface $h(a,b)$ cross that for $\eta(a,b)$ at exactly one point).

3) Simulation example: Let us revisit the simulation example considered in Section III-A.2 and apply the Viviani-curve-based algorithm. For $n = 4$ we obtain $a = 0.1495$m, $b = 0.0072$m and $\theta = -0.1491$(rad). The evolution of the

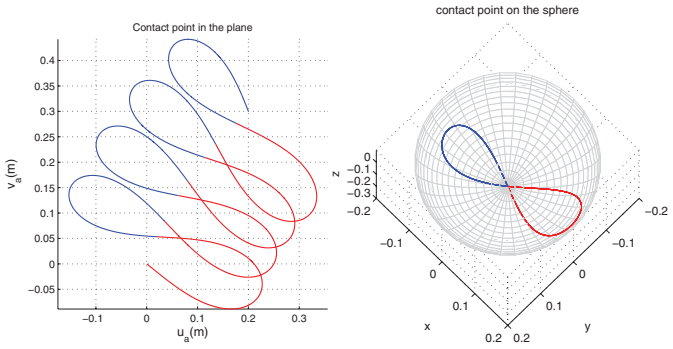

Fig. 10. Trajectory of the contact point on the plane (left) and on the sphere (right); 1st half-step is shown in red, while 2nd in blue color.

contact point on the contact plane and on the hemisphere is shown in Figure 10. The whole maneuver is executed by tracing four times one Viviani's curve on the hemisphere.

In practical calculations the definition of a and b may seem to be involved but in our opinion it is computationally feasible. With a good guess on the initial values of these parameters (that can be obtained from Fig. 9) in our software implementation[2] the solution is obtained relatively fast, within a few seconds.

IV. Conclusions

Motion planning for the rolling-based systems with limited contact area has been discussed in this paper. In particular, we have posed a hybrid parallel parking problem and analyzed two motion planning algorithms based on tracing, respectively, circles and the generalized Viviani curves. In these algorithms, given the initial and final position of the object, the trajectory of the contact point is obtained in several steps. The feasibility of the proposed motion-planning algorithms has been verified under simulation. The circle-based algorithm is very simple but cannot be used when generating C^∞ trajectories in the time domain is required. The Viviani curves-based algorithm does not suffer from this disadvantage but comes with a price of heavier (but still feasible) computations.

The future research should address the issue of controlling the system along the planned trajectories, taking into consideration dynamic effects. In our current formulation the construction of nominal trajectories in the contact coordinates is a purely geometric problem. It should be noted that the extension of the proposed motion planning algorithms to dynamic domain is a very challenging problem. In this connection, the insight gained in the kinematic analysis can be helpful for attacking the motion planning problem in the dynamic formulation.

Acknowledgments

The authors would like to thank Prof. Makoto Kaneko and Dr. Kensuke Harada for interesting discussions and valuable considerations.

[2]We used *Mathematica* system for programming.

References

[1] A. Bicchi, A. Balluchi, D. Prattichizzo, and A. Gorelli, "Introducing the "sphericle": an experimental testbed for research and teaching in nonholonomy," in *Proc. IEEE Int. Conference on Robotics and Automation*, vol. 3, Albuquerque, New Mexico, April 21–27 1997, pp. 2620–2625.

[2] C. Camicia, F. Conticelli, and A. Bicchi, "Nonholonomic kinematics and dynamics of the sphericle," in *Proc. IEEE/RSJ Int. Conference on Intelligent Robots and Systems, IROS'2000*, Takamatsu, Japan, October 30 - November 5 2000, pp. 805–810.

[3] S. Bhattacharya and S. Agrawal, "Spherical rolling robot: A design and motion planning studies," *IEEE Transactions on Robotics and Automation*, vol. 16, no. 6, pp. 835–839, December 2000.

[4] A. Javadi and P. Mojabi, "Introducing glory: A novel strategy for an omnidirectional spherical rolling robot," *ASME Journal of Dynamic Systems, Measurement, and Control*, vol. 126, no. 3, pp. 678–683, September 2004.

[5] R. Balasubramanian, A. Rizzi, and M. Mason, "Legless locomotion for legged robots," The Robotics Institute, Carnegie Mellon University, Tech. Rep. CMU-RI-TR-04-05, 2003.

[6] ——, "Toward legless locomotion control," in *Proc. IEEE/RSJ Int. Conference on Intelligent Robots and Systems,*, vol. 3, Beijing, China, October 9–15 2006, pp. 5594–5599.

[7] Z. Li and J. Canny, "Motion of two rigid bodies with rolling constraint," *IEEE Trans. on Robotics and Automation*, vol. 6, no. 1, pp. 62–72, 1990.

[8] A. Bicchi, A. Marigo, and D. Prattichizzo, "Robotic dexterity via nonholonomy," in *Control Problems in Robotics and Automation*, ser. LNCIS 230, B. Siciliano and K. Valavanis, Eds. Berlin Heidelberg, Germany: Springer Verlag, 1997, pp. 35–49.

[9] A. Bicchi and R. Sorrentino, "Dextrous manipulation through rolling," in *Proc. IEEE Int. Conference on Robotics and Automation*, vol. 1, Nagoya, Japan, May 1995, pp. 452–457.

[10] A. De Luca, G. Oriolo, M. Vendittelli, and S. Iannitti, "Planning motions for robotic systems subject to differential constraints," in *Advances in Control of Articulated and Mobile Robots*, B. Siciliano, A. De Luca, C. Melchiorri, and G. Casalino, Eds. Berlin: Springer Verlag, 2004, pp. 1–38.

[11] G. Oriolo and M. Vendittelli, "Dynamic control of 3-d rolling contacts in two-arm manipulation," *IEEE Transactions on Robotics*, vol. 21, no. 2, pp. 162–175, 2005.

[12] R. Murray, Z. Li, and S. Sastry, *A Mathematical Introduction to Robotic Manipulation*. Boca Raton: CRC Press, 1994.

[13] R. Mukherjee, M. Minor, and J. Pukrushpan, "Motion planning for a spherical mobile robot: Revisiting the classical ball-plate problem," *ASME Journal of Dynamic Systems, Measurement and Control*, vol. 124, no. 4, pp. 502–511, 2002.

[14] A. Marigo and A. Bicchi, "Rolling bodies with regular surface: Controllability theory and applications," *IEEE Trans. on Automatic Control*, vol. 45, no. 9, pp. 1586–1599, September 2000.

[15] A. Bicchi and A. Marigo, "Dexterous grippers: Putting nonholonomy to work for fine manipulation," *Int. Journal of Robotics Research*, vol. 21, no. 5-6, pp. 427–442, May-June 2002.

[16] A. Bicchi, Y. Chitour, and A. Marigo, "Reachability and steering of rolling polyhedra: A case study in discrete nonholonomy," *IEEE Trans. on Automatic Control*, vol. 49, no. 5, pp. 710–726, May 2004.

[17] K. Harada, T. Kawashima, and M. Kaneko, "Rolling based manipulation under neighborhood equilibrium," *The International Journal of Robotics Research*, vol. 21, no. 5-6, pp. 463–474, 2002.

[18] A. Marigo and A. Bicchi, "A local-local planning algorithm for rolling objects," in *Proc. IEEE Int. Conference on Robotics and Automation*, vol. 3, Washington, DC, May 11–15 2002, pp. 1759–1764.

[19] A. Nakashima, K. Nagase, and Y. Hayakawa, "Control of a sphere rolling on a plane with constrained rolling motion," in *Proc. IEEE Conf. on Decision and Control*, vol. 3, Seville, Spain, December 12–25 2005, pp. 1445–1452.

[20] M. Svinin and S. Hosoe, "Simple motion planning algorithms for ball-plate systems with limited contact area," in *Proc. IEEE Int. Conference on Robotics and Automation*, vol. 3, Orlando, Florida, May 15-19 2006, pp. 1755–1761.

[21] D. Montana, "The kinematics of contact and grasp," *The International Journal of Robotics Research*, vol. 7, no. 3, pp. 17–32, 1988.